Electronic Supplementary Material (ESI) for Green Chemistry.

Supporting information

Calix[8]arene-Constructed Stable Polyoxo-Titanium Cluster for Efficient CO_2 Photoreduction

Ning Li,[a†] Jing-Jing Liu,[b†] Jia-Wei Sun,[b] Bao-Xia Dong,[a*] Long-Zhang Dong,[b] Su-Juan Yao,[b] Zhifeng Xin,[c] Shun-Li Li[b] and Ya-Qian Lan[b*]

[a]School of Chemistry and Chemical Engineering, Yangzhou University, Yangzhou 225002 (P. R. China). E-mail: bxdong@yzu.edu.cn.

[b]Jiangsu Collaborative Innovation Centre of Biomedical Functional Materials, School of Chemistry and Materials Science, Nanjing Normal University No.1, Wenyuan Road, NanJing 210023 (China). E-mail: yqlan@njnu.edu.cn.

[c]Institute of Molecular Engineering and Applied Chemistry, Anhui University of Technology, Ma'anshan, Anhui, 243002, PR China

[†]These authors contributed equally to this work.

Materials and General Methods

Photocatalytic Reaction

Photocatalytic reduction of CO_2 was performed in a 100 mL quartz reactor with as-prepared crystal. Photocatalyst (5mg) was added into the solution which contained deionized H_2O (24 mL) and triethanolamine (TEOA, 6 mL) as an electron donor. After degassing with CO_2 to remove dissolved O_2 for 20 min, the UV light-driven photocatalytic reaction was performed under the irradiation of a 300 W Xe lamp with UV and IR-cut to keep the wavelengths in the range from 200 to 400 nm. For visible light-driven photocatalytic reaction, a 300 W xenon arclamp (light intensity: 200 mW cm^{-2}) with a cut filter (to ensure effective wavelengths are in the range of 420 to 800 nm) was used as light source. The reaction temperature was controlled at 303 K by using the cooling water circulation. In order to detect the content of carbon monoxide produced by the reaction mixture, 500 μL of gas-product was extracted from the reactor with a syringe and injected into the gas chromatograph with a FID detector, using nitrogen as the carrier gas and reference gas. To detect the formation of hydrogen from the reaction mixture, 500 μL from the middle of the reactor was taken out with a syringe and injector into a GC with a TCD detector, using nitrogen as the carrier gas and reference gas. By comparing the integrated area of the gas-phase product with the calibration curve, the volume of carbon monoxide and hydrogen can be calculated. All photocatalytic reactions were repeated five times to ensure the accuracy of the experimental data.

Photoelectrochemical measurements

Photoelectrochemical measurements were carried out on CHI 660e electrochemical workstation in a standard three-electrode electrochemical cell with a working electrode, a platinum plate as counter electrode and a saturated Ag/AgCl electrode as reference electrode. A sodium sulfate solution

(0.2 M) was used as the electrolyte.

Preparation of the working electrode: 2 mg crystals powder was mixed with 0.99 mL ethanol and 10 μl Nafion D-520 dispersion solutions and sonicated for 30 minutes. The resulting mixture was deposited evenly on the bottom 1 × 2 cm^2 area of the ITO glass plates and left in the air to dry.

Preparation of working electrode for electrochemical impedance spectroscopy (EIS): The as-synthesized crystals (10 mg) were grinded to powder and then dispersed in 1mL solvent (900μL H_2O and 100 μL 5wt% Nafion) by ultrasonication to form a homogeneous ink. Subsequently, 50 μL of the ink was covered onto the both side of carbon cloth for EIS test.

Crystallographic information

Table S1a. Crystal data and structure refinement for **Ti_4-C8A** and **Ti_7-C8A**.

Compound	**Ti_4-C8A**	**Ti_7-C8A**
Empirical formula	$C_{71}H_{76}O_{15}Ti_4$	$C_{68}H_{76}O_{24}Ti_7$
M_r (g mol^{-1})	1360.92	1612.38
Crystal system	Monoclinic	Orthorhombic
Space group	$P2_1/n$	$Cmc2_1$
a (Å)	18.731(8)	24.63(3)
b	16.579(7)	19.10(3)
c	21.872(10)	14.90(2)
α (°)	90	90
β (°)	100.786(6)	90
γ (°)	90	90
V (Å^3)	6672(5)	7010(17)
Z	4	4
D_{calcd} (g cm^{-3})	1.354	1.528
R (int)	0.0714	0.0841
μ	0.527	0.835
F (000)	2836.0	3320.0
R_1 [$I > 2\sigma(I)$]^a	0.0677	0.0827
wR_2 [$I > 2\sigma(I)$]^b	0.1447	0.1572
R_1 (all data)	0.1416	0.1604
wR_2 (all date)	0.1766	0.1938
GOF on F^2	1.028	1.120

$^aR_1 = \sum||F_o| - |F_c||/|F_o|$. $^bwR_2 = [\sum w(F_o^2 - F_c^2)^2/\sum w(F_o^2)^2]^{1/2}$.

Table S1b. Selected bond lengths (Å) and angles (°) for **Ti_4-C8A** and **Ti_7-C8A**.

Ti_4-C8A			
Ti1-O1	1.828(3)	O1-Ti1-O2	79.96(14)
Ti1-O2	2.160(3)	O1-Ti1-O9	136.65(15)
Ti1-O8	1.828(3)	O8-Ti1-O2	158.74(15)
Ti1-O9	1.934(3)	O2-Ti2-O9	74.78(12)
Ti1-O11	1.745(4)	O3-Ti2-O2	92.89(14)
Ti2-O2	1.958(3)	O3-Ti2-O10	95.80(14)
Ti2-O3	1.805(3)	O3-Ti2-O9	150.06(15)
Ti2-O9	2.029(3)	O7-Ti3-O6	93.45(14)
Ti2-O10	1.914(3)	O7-Ti3-O9	93.80(14)
Ti2-O12	1.753(4)	O7-Ti3-O10	150.75(15)
Ti3-O6	1.967(3)	O9-Ti3-Ti4	108.90(10)
Ti3-O7	1.787(3)	O4-Ti4-O5	95.78(14)
Ti3-O9	1.945(3)	O4-Ti4-O6	172.29(15)
Ti3-O10	1.985(3)	O4-Ti4-O10	106.29(13)
Ti4-O4	1.838(3)	O4-Ti4-O15	86.42(17)
Ti4-O5	1.845(3)	O5-Ti4-O6	82.58(12)
Ti4-O6	2.185(3)	O5-Ti4-O10	150.17(13)
Ti4-O10	1.974(3)	O6-Ti4-Ti3	36.95(7)
Ti4-O14	1.813(3)	O10-Ti4-O6	72.85(11)
Ti4-O15	2.313(4)	O14-Ti4-O4	97.80(15)
Ti_7-C8A			
Ti1-O7	2.037(9)	O7-Ti2-O12	78.4(5)
Ti1-O5	1.992(8)	O6-Ti2-Ti2	137.5(3)

Ti1-O1	1.841(9)	O6-Ti2-Ti4	138.0(4)
Ti1-O10	2.051(10)	O6-Ti2-Ti3	186.3(3)
Ti1-O8	1.958(11)	O6-Ti2-Ti3	86.3(3)
Ti1-O2	1.789(10)	O6-Ti2-O7	97.0(4)
Ti2-O7	2.014(9)	O6-Ti2-O12	75.4(4)
Ti2-O6	2.003(9)	O4-Ti2-Ti21	92.6(3)
Ti2-O4	1.817(9)	O4-Ti2-Ti4	128.6(4)
Ti2-O12	2.021(10)	O4-Ti2-Ti3a	132.2(4)
Ti2-O3	1.829(10)	O4-Ti2-Ti3	132.2(4)
Ti2-O9	1.968(11)	O4-Ti2-O7	167.6(4)
Ti3-O7	2.062(10)	O4-Ti2-O6	92.2(5)
Ti3-O7a	2.061(10)	O4-Ti2-O12	96.0(5)
Ti3-O11	1.829(11)	O4-Ti2-O3	97.4(4)
Ti3-O11a	1.829(11)	O4-Ti2-O9	91.0(4)
Ti3-O12	1.945(14)	O12-Ti2-Ti2	138.1(4)
Ti3-O10	1.972(14)	O12-Ti2-Ti4	88.9(4)
Ti4-O7	2.109(10)	O12-Ti2-Ti3	37.6(4)
Ti4-O11a	2.062(12)	O12-Ti2-Ti3	137.6(4)
Ti4-O14	1.786(11)	O3-Ti2-Ti2a	129.7(3)
Ti4-O13	1.742(11)	O3-Ti2-Ti4	91.5(3)
Ti4-O8	1.998(10)	O3-Ti2-Ti3	130.4(3)
Ti4-O9	2.008(10)	O3-Ti2-Ti3a	130.4(3)

Symmetry transformations used to generate equivalent atoms:

Ti$_7$-C8A: a (1-X,+Y,+Z)

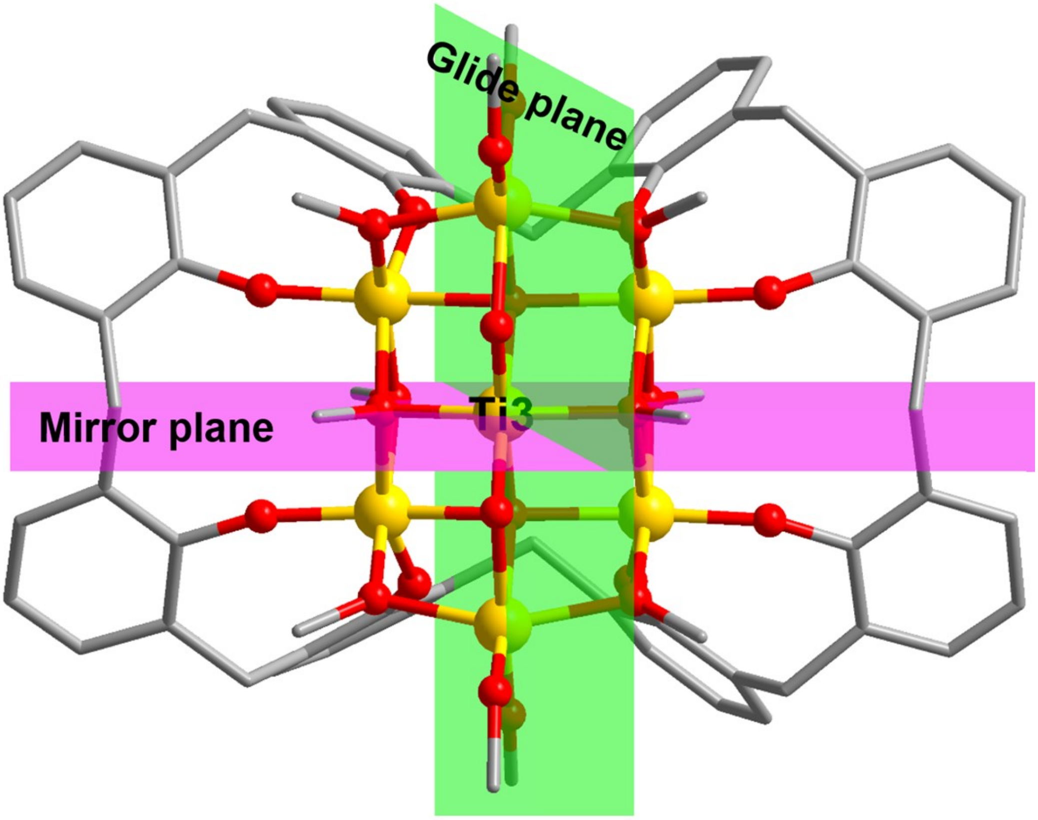

Figure S1. Within the metal-oxo core of **Ti_7-C8A**, Ti3 atom is located at the intersection of symmetric elements of glide and mirror planes.

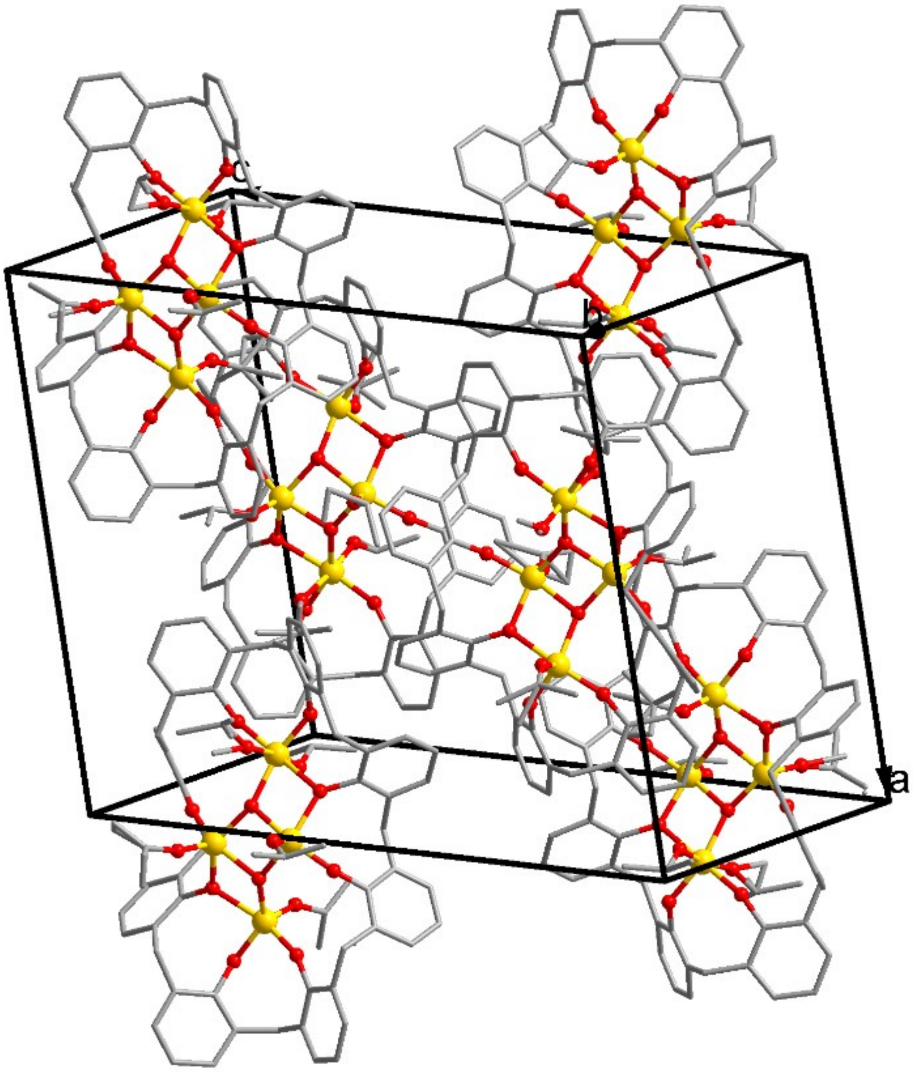

Figure S2. Three-dimensional supramolecular stacking of **Ti_4-C8A** clusters.

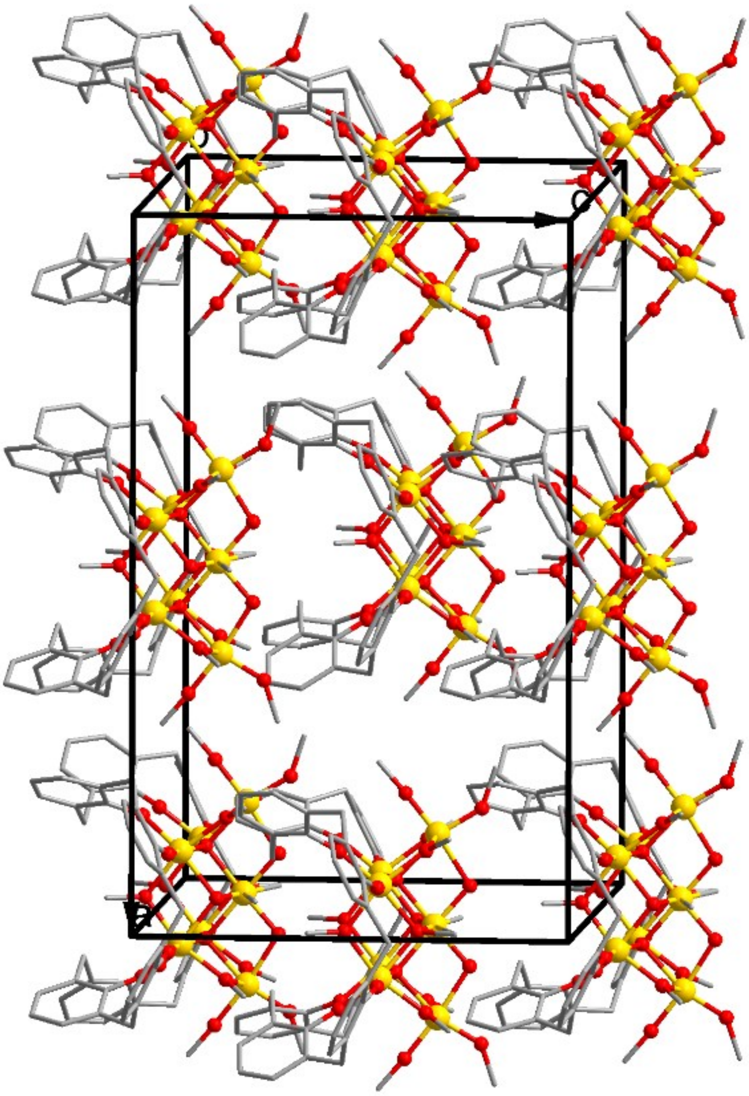

Figure S3. Three-dimensional supramolecular stacking of **Ti$_7$-C8A** clusters.

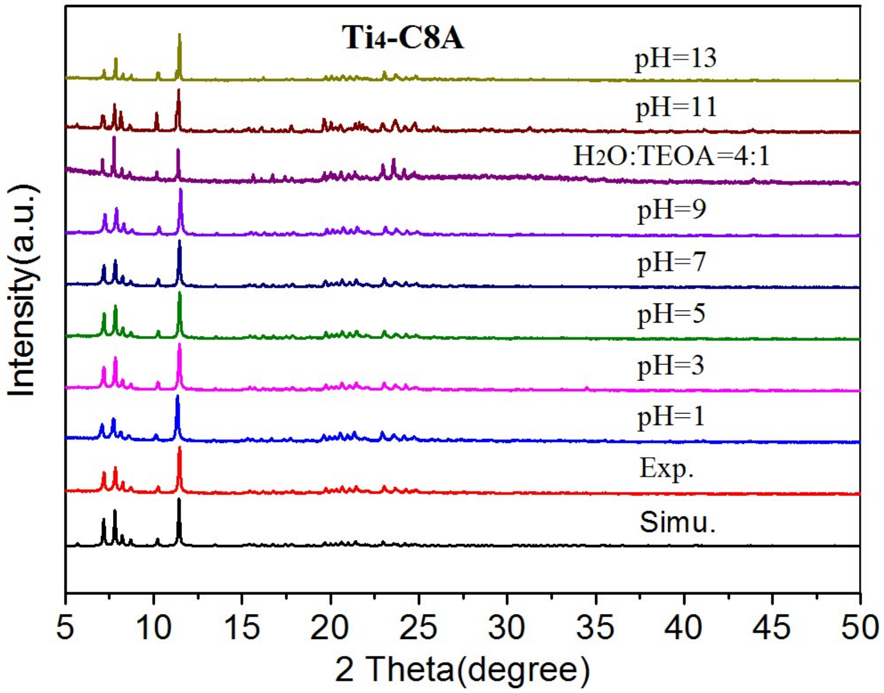

Figure S4. PXRD patterns of the as-synthesized and simulated **Ti_4-C8A**. The chemistry stability of **Ti_4-C8A** was confirmed by the obtained well-matched PXRD patterns (compared with the simulated PXRD pattern) after immersing crystals into aqueous solutions with different pH values and reaction solution for one week.

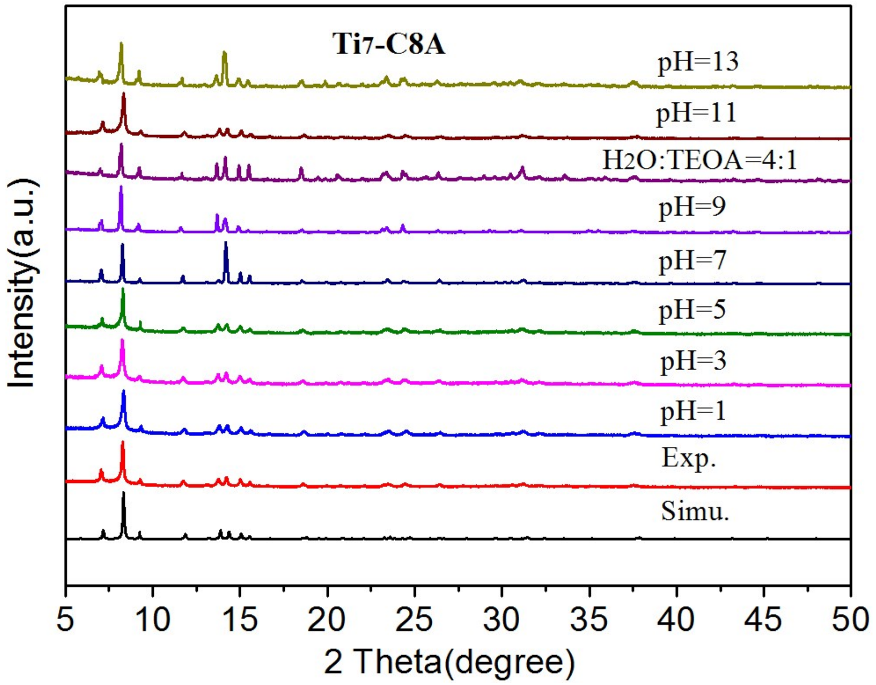

Figure S5. PXRD patterns of the as-synthesized and simulated **Ti_7-C8A**. The chemistry stability of **Ti_7-C8A** was confirmed by the obtained well-matched PXRD patterns (compared with the simulated PXRD pattern) after immersing crystals into aqueous solutions with different pH values and reaction solution for one week.

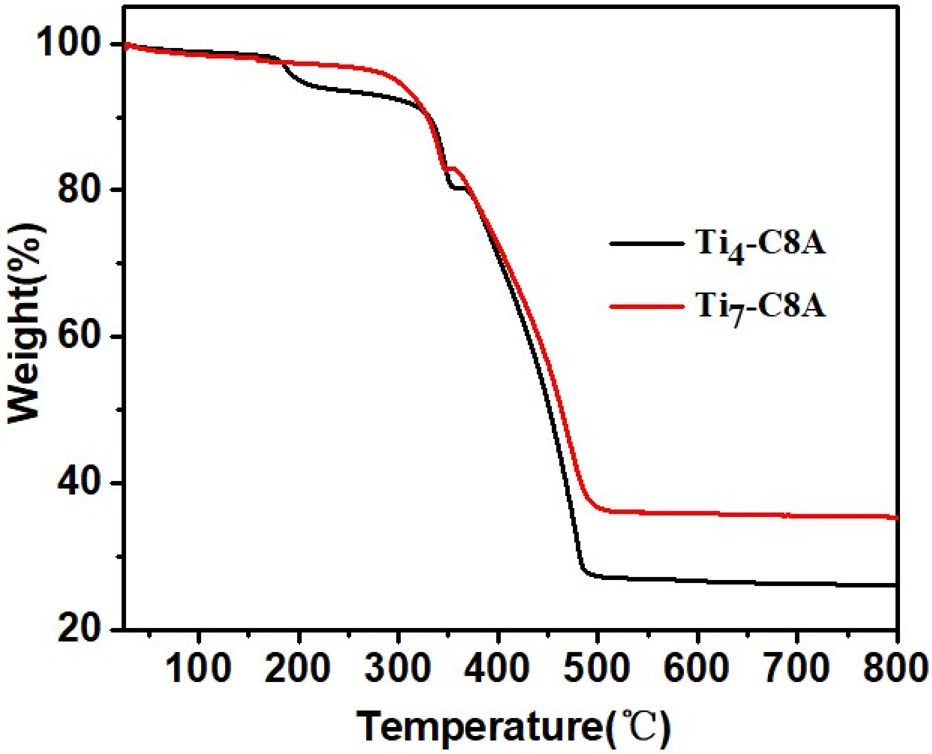

Figure S6. Thermal gravimetrical analysis of **Ti_4-C8A** (black) and **Ti_7-C8A** (red).

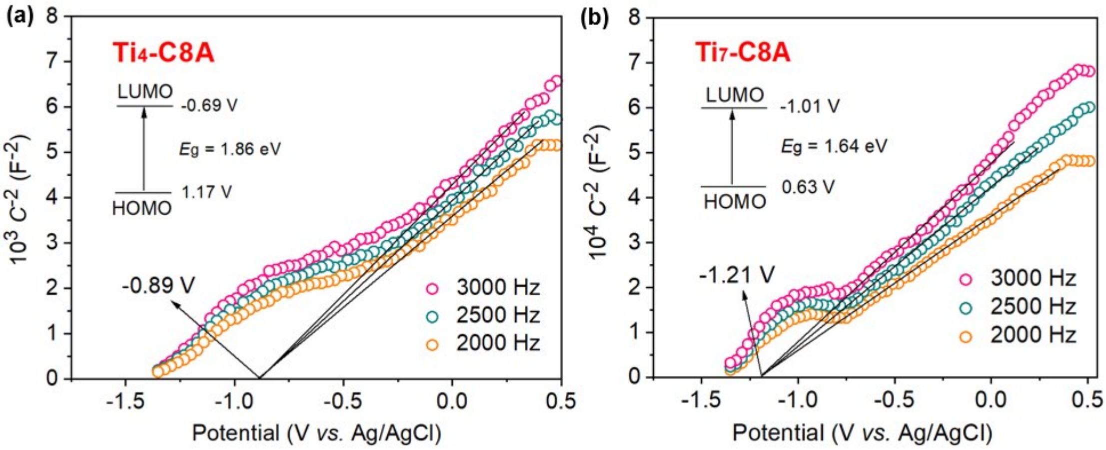

Figure S7. Mott-Schottky plots of **Ti_4-C8A** and **Ti_7-C8A** with inset of energy diagram of the LUMO and HOMO levels.

To further confirm the HOMO and LUMO levels of **Ti_4-C8A** and **Ti_7-C8A**, the Mott–Schottky measurements were conducted. As shown in Figure S7, we can see that the LUMO positions of **Ti_4-C8A** and **Ti_7-C8A** were evaluated to be -0.69 (*vs.* NHE, pH = 7) and -1.01 V(*vs.* NHE, pH = 7), respectively, while the HOMO levels were evaluated to be 1.17 V (**Ti_4-C8A**, *vs.* NHE, pH = 7) and 0.63 V (**Ti_7-C8A**, *vs.* NHE, pH = 7). It is obvious that the calculated HOMO and LUMO values from Mott–Schottky measurements are very close to the results extracted from UPS, and the difference is inevitable because of different characterization methods. Thus, the LUMO potentials of **Ti_4-C8A** and **Ti_7-C8A** should be in the range of -0.69 to -0.74 V (*vs.* NHE, pH = 7) and -0.98 to -1.01 V (*vs.* NHE, pH = 7), respectively, while their HOMO potentials are in the range of 1.12 to 1.17 V and 0.63 to 0.66 V. Based on the above results, we can find that the determined LUMO potentials of **Ti_4-C8A** and **Ti_7-C8A** are all more negative than the standard reduction potential of CO_2/HCOOH (-0.61 V *vs.* NHE, pH = 7). Therefore, both of **Ti_4-C8A** and **Ti_7-C8A** can catalyze the reduction of CO_2 to $HCOO^-$.

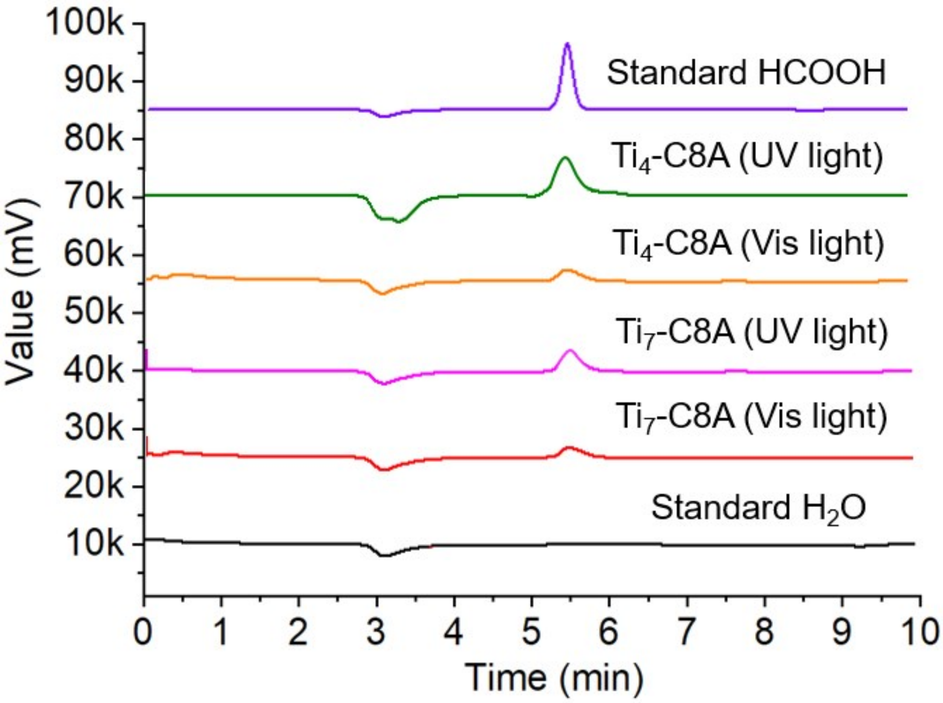

Figure S8. Analysis of the liquid reaction products generated in photocatalytic system by ion chromatography.

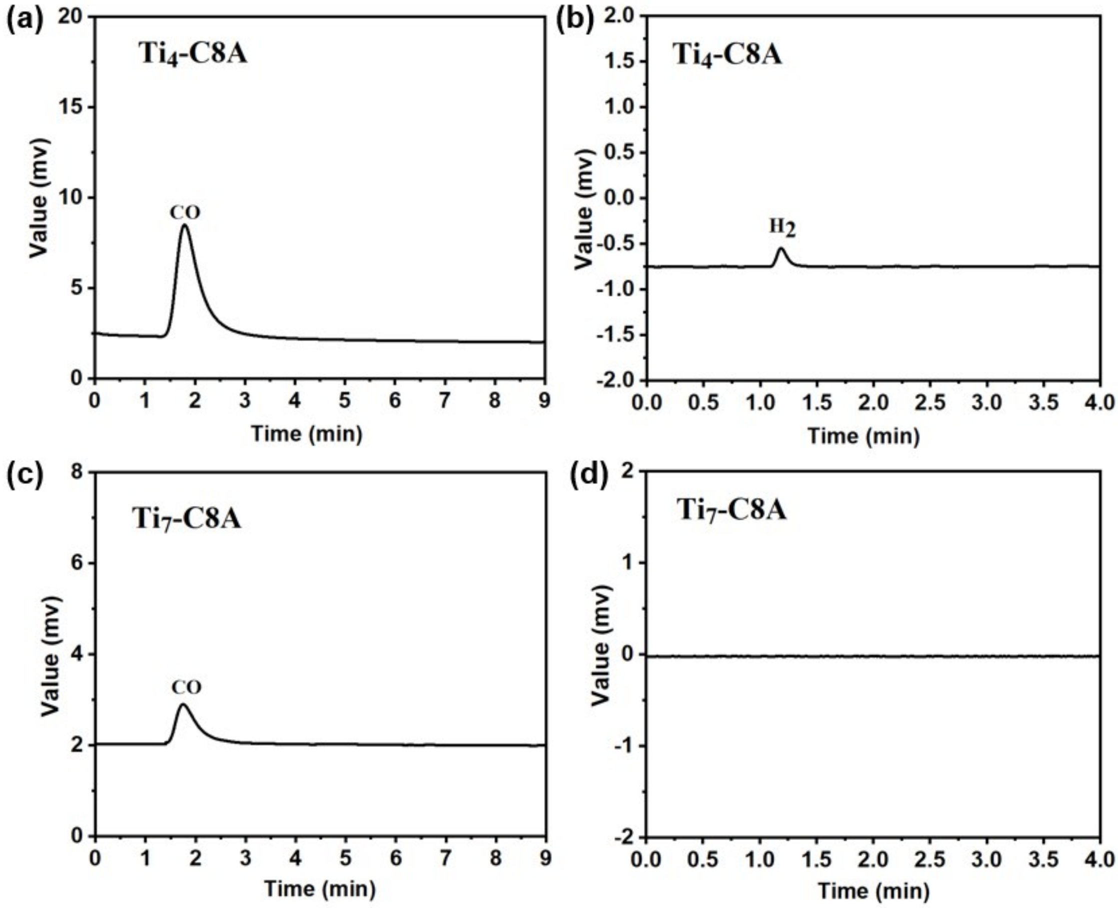

Figure S9. The signals in gas chromatography during the UV light-driven photocatalytic reaction. Trace amount of competitive H_2 and CO were observed for (a,b) **Ti_4-C8A**, whereas only trace amount of CO was observed for (c,d) **Ti_7-C8A**.

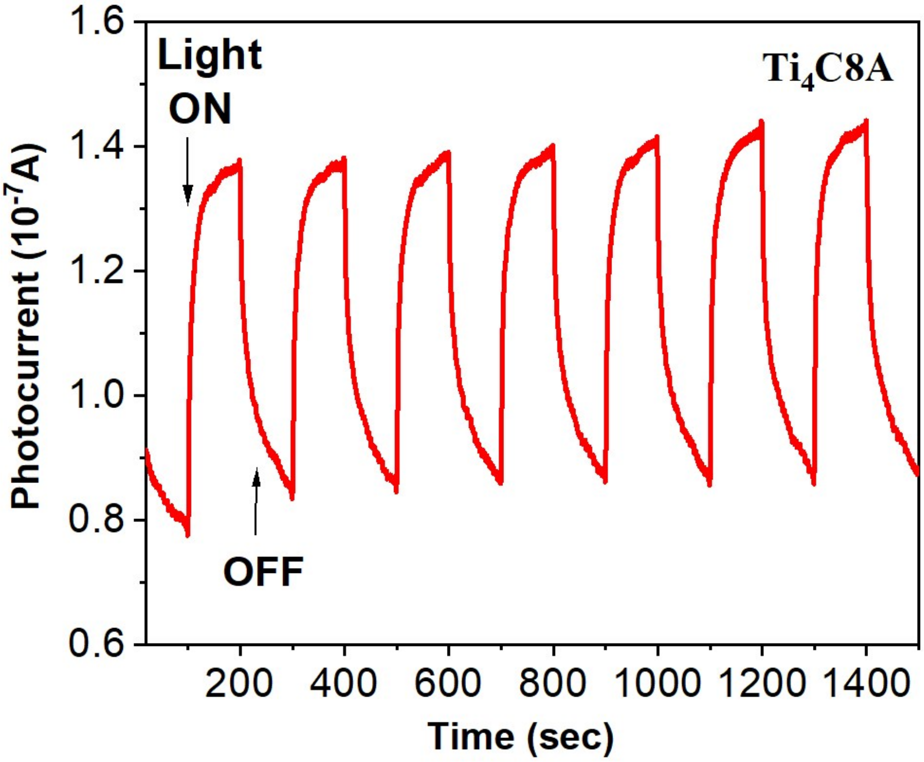

Figure S10. Transient photocurrent response (UV light) of **Ti$_4$-C8A**.

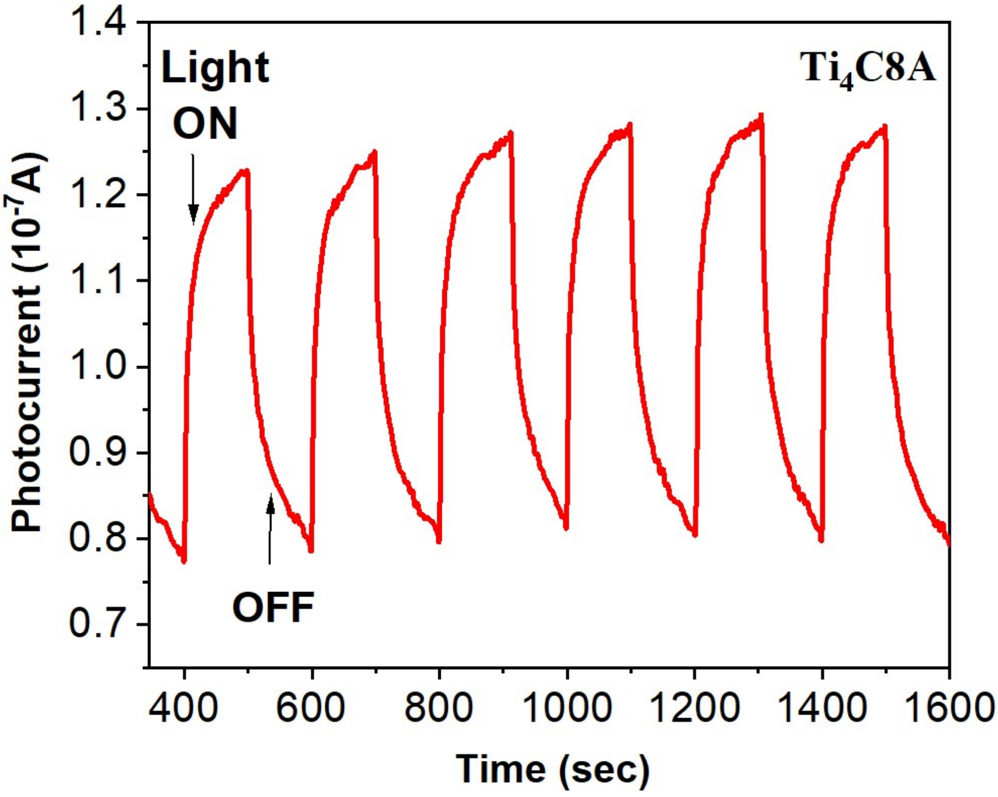

Figure S11. Transient photocurrent response (visible light) of **Ti$_4$-C8A**.

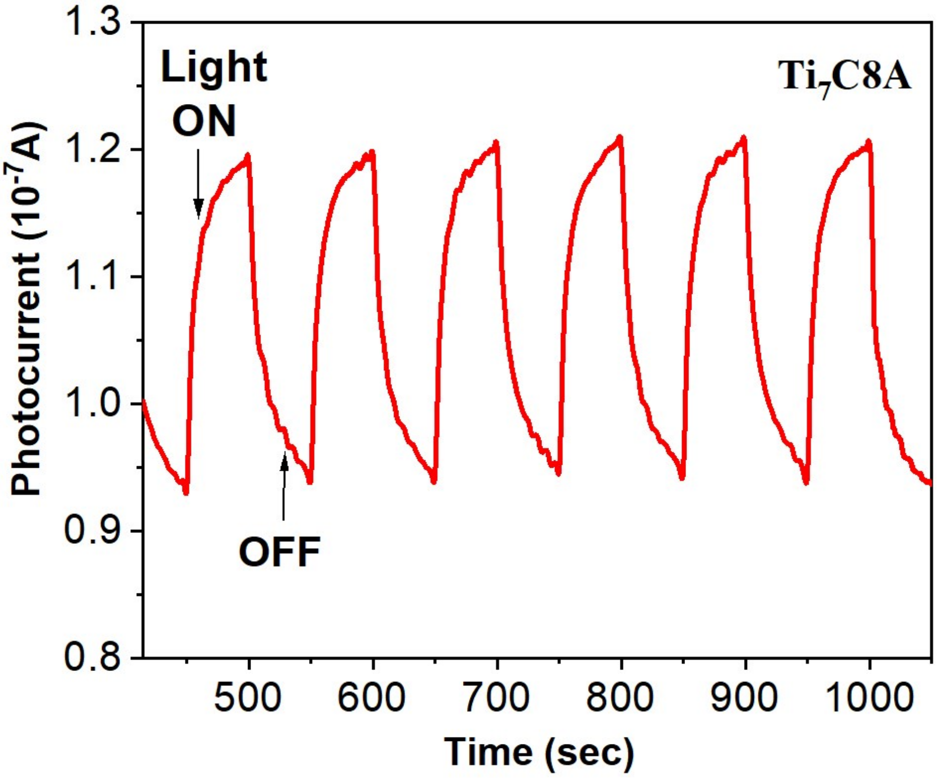

Figure S12. Transient photocurrent response (UV light) of **Ti$_7$-C8A**.

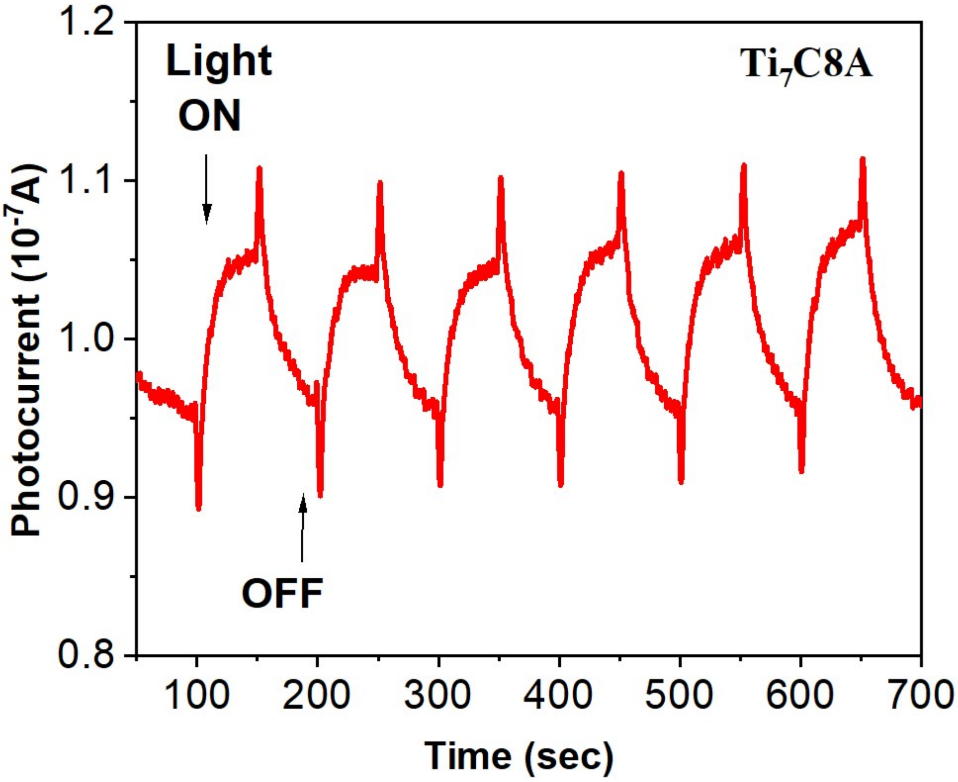

Figure S13. Transient photocurrent response (visible light) of **Ti$_7$-C8A**.

To investigate the electrochemical properties of the as-obtained catalyst, electrochemical impedance spectroscopy (EIS) was performed on an electrochemical workstation (Bio-Logic) with a standard three-electrode system in a frequency range from 1000 kHz to 100 mHz at ambient environment. The carbon cloth (CC, 1 cm×1 cm) modified with catalyst samples, platinum wire and Ag/AgCl (saturated) were used as working electrode, counter electrode and reference electrode, respectively and 0.5 M $KHCO_3$ aqueous solution was used as the supporting electrolyte. As shown in Figure S14, the size of the Nyquist plot of **Ti_7-C8A** is smaller than that of **Ti_4-C8A**, which represents the interfacial charge transfer process of **Ti_7-C8A** is faster compared to **Ti_4-C8A**.

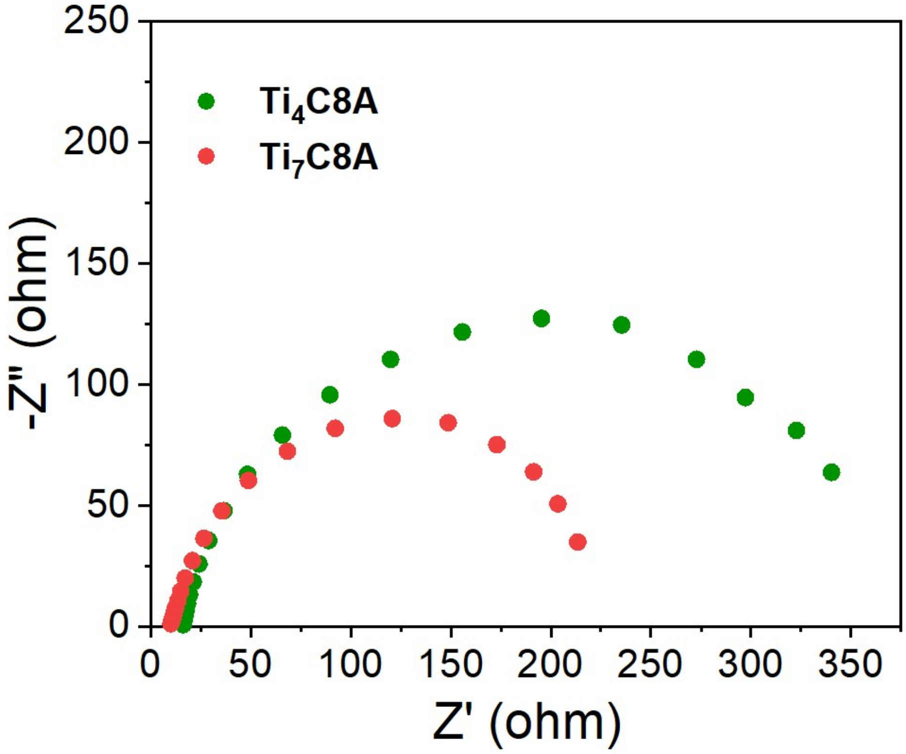

Figure S14. Nyquist plots of catalysts over the frequency ranging from 1000 kHz to 100 mHz.

Calculation

To further validate the exciton separation (or charge separation) efficiency of Ti_4-C8A and Ti_7-C8A, we calculated the electron-hole Coulomb attraction energies (E_c) in the first excited state. In general, the small E_c leads to high exciton separation efficiency. The density functional theory (DFT) and time-dependent (TD-DFT) were employed in this work. Structure optimizations were performed without constraints using PBE0 functional and Def2SVP basis set. The solvent effect was considered using SMD model, water as the solvent. All DFT and TD-DFT calculations were carried out using Gaussian 16 A.[1] The electron-hole analysis was performed using Multiwfn3.7.[2] Calculated E_c values are 3.42 and 2.16 eV for Ti_4-C8A and Ti_7-C8A, respectively (Figure S15). This result also suggested that Ti_7-C8A has higher exciton separation efficiency than Ti_4-C8A, which is consistent with our experimental data.

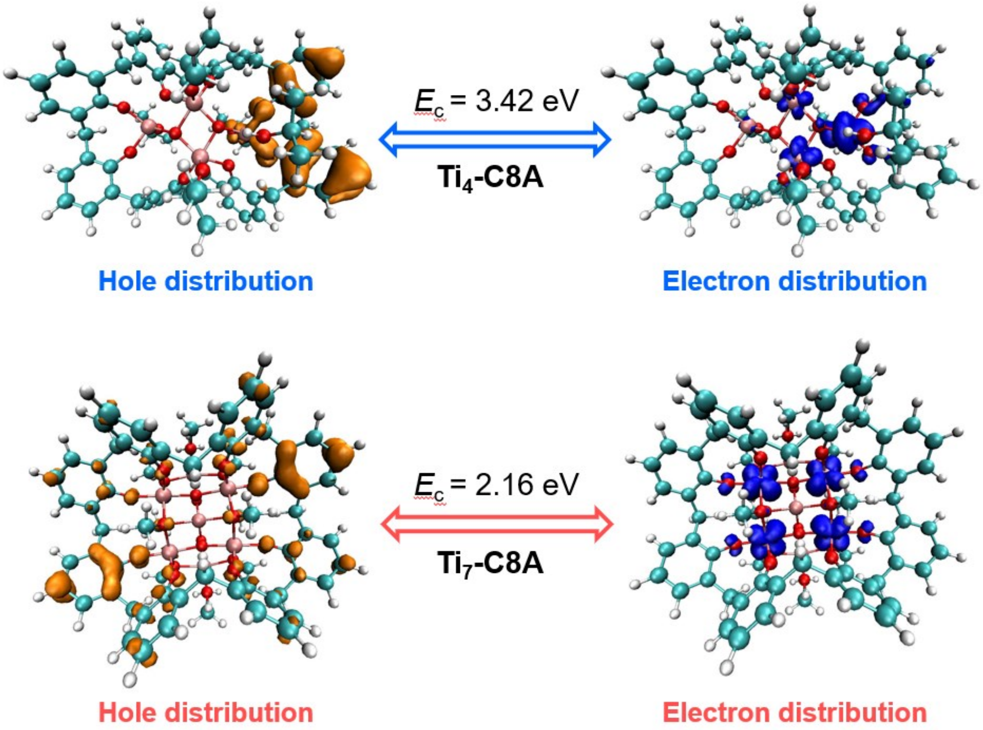

Figure S15. Calculations of electron-hole Coulomb attraction energies (E_c) in the first excited state for **Ti_4-C8A** and **Ti_7-C8A**.

Turnover number (TON) Calculation

From structurally, we assume that the potentially active sites (Ti1, Ti2, Ti3, Ti4 atoms) in **Ti_4-C8A** is twice that (two Ti4 atoms) of **Ti_7-C8A**. Therefore, we have compared the catalytic activity of active sites in **Ti_4-C8A** and **Ti_7-C8A** by turnover number (TON).

Turnover number (TON) = mol ($HCOO^-$ yield) / mol (catalyst)

Turnover number (TON_{Ti}) = mol ($HCOO^-$ yield) / mol (Ti^{4+} active sites)

mol (Ti^{4+} active sites) = g (Ti_4-C8A catalyst, mass) / $g \cdot mol^{-1}$ (Ti_4-C8A catalyst, M_r) × 4

mol (Ti^{4+} active sites) = g (Ti_7-C8A catalyst, mass) / $g \cdot mol^{-1}$ (Ti_7-C8A catalyst, M_r) × 2

Table S2. The catalytic activity comparison of potential active sites in **Ti_4-C8A** and **Ti_7-C8A**.

Entry	($HCOO^-$ yield) (*UV* light)	TON	TON_{Ti}	($HCOO^-$ yield) (*Visible light*)	TON	TON_{Ti}
Ti_4-C8A	41.51 *μ*mol	11.3	2.8	8.25 *μ*mol	2.3	0.6
Ti_7-C8A	21.58 *μ*mol	7.0	3.5	6.19 *μ*mol	2.0	1.0

From the calculated catalytic activity data, each potential Ti^{4+} catalytic site (TON_{Ti}) in **Ti_7-C8A** is more active than that of **Ti_4-C8A** under UV or visible light irradiation, whereas the **Ti_4-C8A** cluster has a higher overall TON. Therefore, the higher photocatalytic activity of **Ti_4-C8A** compared with **Ti_7-C8A** is mainly attributed to its more potential active Ti^{4+} sites.

Table S3. Comparison of the photocatalytic performance of **Ti_4-C8A**, **Ti_7-C8A**, and reported heterogeneous nanostructured and crystalline photocatalysts for CO_2-to-HCOOH conversion.

Photocatalyst	**Solvent**	**Light source**	**PS/PM**	**HCOOH (μmol/g/h) (selec.%)**	**Quantum efficiency (QE) for HCOOH**	**Reference**
	Coordination molecular complexes photocatalysts (This work)					
Ti_4-C8A	H_2O	300 W Xe-lamp, UV light (200-400 nm)	No	488.35 (96.0%)	0.016% (365 nm)	this work
Ti_4-C8A	H_2O	300 W Xe-lamp, Visible light (420-800 nm)	No	97.06 (100%)	0.013% (420 nm) 0.011% (450 nm)	this work
Ti_7-C8A	H_2O	300 W Xe-lamp, UV light (200-400 nm)	No	253.88 (99.7%)	0.008% (365 nm)	this work
Ti_7-C8A	H_2O	300 W Xe-lamp, Visible light (420-800 nm)	No	72.82 (100%)	0.003% (420 nm) 0.002% (450 nm) 0.001% (500 nm)	this work
	Nanostructured semiconductor photocatalysts					
TiO2/Cu(II) phthalocyanine	H_2O	halogen lamp	No	26.05 (100%)	----	[3]
3.0 wt % Cu-doped anatase TiO2	H_2O	125 W Hg-lamp (λ = 365 nm)	No	25.6 (ca. 10.9%)	----	[4]
Bi2S3	MeOH	250 W Hg-lamp (λ = 365 nm)	No	175	----	[5]
CdIn2S4	MeOH	250 W Hg-lamp (λ = 365 nm)	No	1428.5	----	[6]
ZnIn2S4	MeOH	250 W Hg-lamp (λ = 365 nm)	No	190.5	----	[7]
SiC	NaOH solution	300 W Xe-lamp	No	12 (90.7%)	----	[8]
N-Doped Ta_2O_5	MeCN	A 400 W high-pressure Hg lamp (> 400 nm)	Yes	70 (<100%)	----	[9]
g-C_3N_4-Re(bbpa)$(CO)_2$Cl$_2$]·$(PF_6)_2$	DMA	A 400 W high-pressure Hg lamp (> 400 nm)	Yes	1100 (100%)	5.7% (400 nm)	[10]
ZnS	Isopropanol/H2O	150 W XBO arc lamp (> 320 nm)	Yes	100 (<100%)	0.50% (375 nm)	[11]
	Metal-organic frameworks (MOFs)-based photocatalysts					
AD-MOF-1	MeCN	300 W Xe-lamp, Visible light (420-800	No	179.0 (100%)	----	[12]

		nm)				
AD-MOF-2	H_2O	300 W Xe-lamp, Visible light (420-800 nm)	No	443.2 (100%)	----	[12]
PCN-222	MeCN	300 W Xe-lamp, Visible light (420-800 nm)	No	60 (100%)	----	[13]
NH_2-MIL-125(Ti)	MeCN	Four 4W UV lamps with a wavelength centered at 365 nm	No	16.28 (100%)	----	[14]
NH_2-MIL-101(Fe)	MeCN	300 W Xe-lamp, Visible light (420-800 nm)	No	445 (100%)	----	[15]
NH_2-MIL-53(Fe)	MeCN	300 W Xe-lamp, Visible light (420-800 nm)	No	116.25 (100%)	----	[15]
NH_2-MIL-88B(Fe)	MeCN	300 W Xe-lamp, Visible light (420-800 nm)	No	75.0 (100%)	----	[15]
UiO-66(Zr/Ti)-NH_2	MeCN	300 W Xe arc lamp, Visible light (420-800 nm)	No	-/(100%)	----	[16]
UiO-66-(Zr/Ti)-NH_2	MeCN	300 W Xe-lamp, Visible light (420-800 nm)	No	5.8 mmol mol^{-1} (100%)	----	[17]
H_2N-UIO-66(Zr)	MeCN	300 W Xe-lamp, Visible light (420-800 nm)	No	26.4 (100%)	----	[18]
NNU-28	MeCN	300 W Xe-lamp, Visible light (> 420 nm)	No	52.8 (100%)	----	[19]
MOF-253, Ru(bpy)$(CO)_2Cl_2$	MeCN	300 W Xe-lamp, Visible light (420-800 nm)	Yes	16.75 (25.5%)	----	[20]
Ru-MOF	MeCN	Xe-lamp, Visible light (420-800 nm)	Yes	71.66/77.18 (100%)	0.67% (475 nm)	[21]

PS: photosensitizer; PM: precious metal.

The QE measurement:

The apparent quantum efficiency (QE) for HCOOH evolution was measured using monochromatic visible light (365 / 420 / 450 / 500 nm). Depending on the amounts of HCOOH produced by the photocatalytic reaction in an average of one hour, and the QE was calculated as follow:

$$QE = \frac{(2 \times the\ number\ of\ HCOOH)\ molecules\ produced}{the\ number\ of\ incident\ photons} \times 100\%$$

$$QE = \frac{2 \times M \times N_A \times h \times c}{S \times P \times T \times \lambda} \times 100\%$$

M = yield of HCOOH (mol);

Monochromatic light (λ)	365 nm	420 nm	450 nm	500 nm
Ti_4-C8A ($HCOO^-$, μmol)	5.93	5.51	5.53	
Ti_7-C8A ($HCOO^-$, μmol)	2.94	1.45	1.16	0.54

N_A (Avogadro constant) = 6.02×10^{23} mol^{-1};
h (Planck constant) = 6.626×10^{-34} J·s;
c (Speed of light) = 3×10^8 m/s;
S = Irradiation area (cm^2) = 7.06 cm^2;
P = the intensity of irradiation light (W / cm^2) = 55.2 mW / cm^2 (365 nm) or 55.4 mW / cm^2 (420 nm) or 59.7 mW / cm^2 (450 nm) or 60.8 mW / cm^2 (500 nm);
T = the photoreaction time (s) = 17 × 3600 = 61200 s;
λ = the wavelength of the monochromatic light (nm) = 365×10^{-9} m / 420×10^{-9} m / 450×10^{-9} m / 500×10^{-9} m.

Quantum Efficiency (QE) for **Ti_4-C8A**:

$$QE\ (365\ nm) = \frac{2 \times 5.93 \times 10^{-6} \times 6.02 \times 10^{23} \times 6.626 \times 10^{-34} \times 3 \times 10^8}{7.06 \times 55.2 \times 10^{-3} \times 61200 \times 365 \times 10^{-9}} \times 100\% = 0.016\%$$

$$QE\ (420\ nm) = \frac{2 \times 5.51 \times 10^{-6} \times 6.02 \times 10^{23} \times 6.626 \times 10^{-34} \times 3 \times 10^8}{7.06 \times 55.4 \times 10^{-3} \times 61200 \times 420 \times 10^{-9}} \times 100\% = 0.013\%$$

$$QE\ (450\ nm) = \frac{2 \times 5.53 \times 10^{-6} \times 6.02 \times 10^{23} \times 6.626 \times 10^{-34} \times 3 \times 10^8}{7.06 \times 59.7 \times 10^{-3} \times 61200 \times 450 \times 10^{-9}} \times 100\% = 0.011\%$$

Quantum Efficiency (QE) for **Ti_7-C8A**:

$$QE\ (365\ nm) = \frac{2 \times 2.94 \times 10^{-6} \times 6.02 \times 10^{23} \times 6.626 \times 10^{-34} \times 3 \times 10^8}{7.06 \times 55.2 \times 10^{-3} \times 61200 \times 365 \times 10^{-9}} \times 100\% = 0.008\%$$

$$QE\ (420\ nm) = \frac{2 \times 1.45 \times 10^{-6} \times 6.02 \times 10^{23} \times 6.626 \times 10^{-34} \times 3 \times 10^{8}}{7.06 \times 55.4 \times 10^{-3} \times 61200 \times 420 \times 10^{-9}} \times 100\% = 0.003\%$$

$$QE\ (450\ nm) = \frac{2 \times 1.16 \times 10^{-6} \times 6.02 \times 10^{23} \times 6.626 \times 10^{-34} \times 3 \times 10^{8}}{7.06 \times 59.7 \times 10^{-3} \times 61200 \times 450 \times 10^{-9}} \times 100\% = 0.002\%$$

$$QE\ (500\ nm) = \frac{2 \times 0.54 \times 10^{-6} \times 6.02 \times 10^{23} \times 6.626 \times 10^{-34} \times 3 \times 10^{8}}{7.06 \times 60.8 \times 10^{-3} \times 61200 \times 500 \times 10^{-9}} \times 100\% = 0.001\%$$

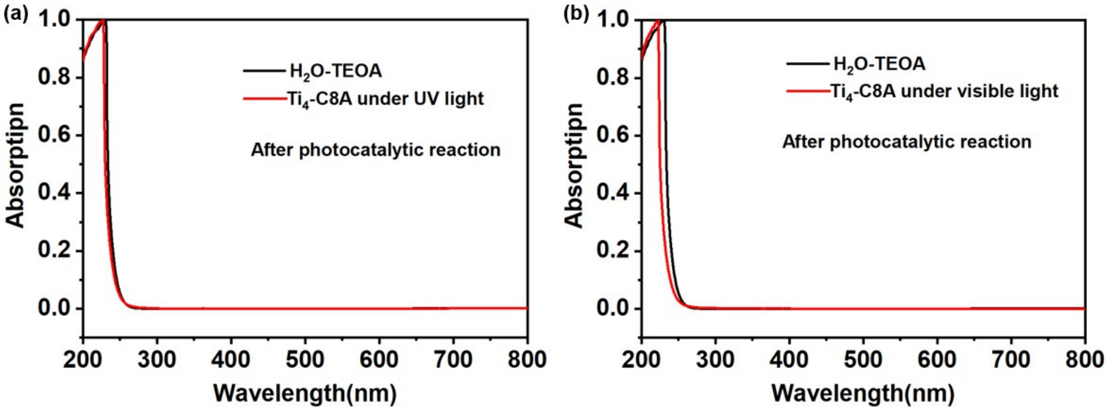

Figure S16. Absorption spectra of filtrate derived from **Ti_4-C8A** reactive solution after photocatalytic reaction. There is no obvious absorption signal appeared, ruling out the influence of the decomposed active component on the photocatalytic reaction.

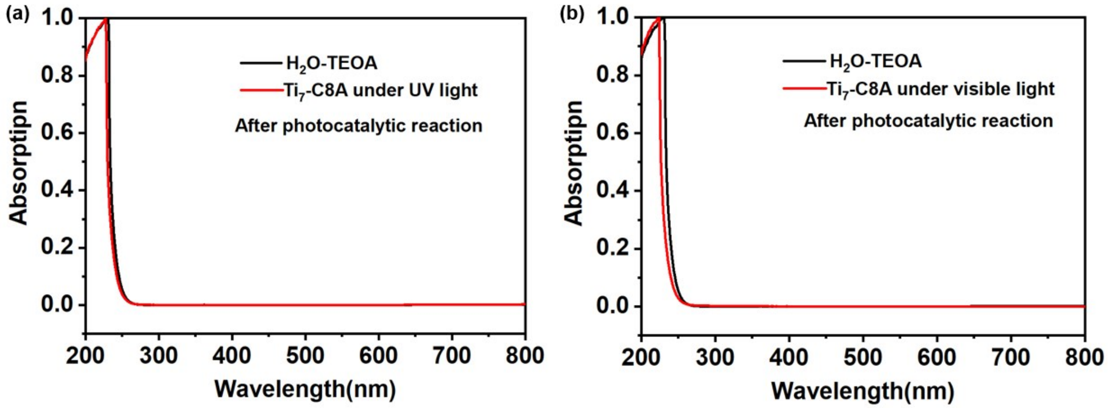

Figure S17. Absorption spectra of filtrate derived from **Ti_7-C8A** reactive solution after photocatalytic reaction. There is no obvious absorption signal appeared, ruling out the influence of the decomposed active component on the photocatalytic reaction.

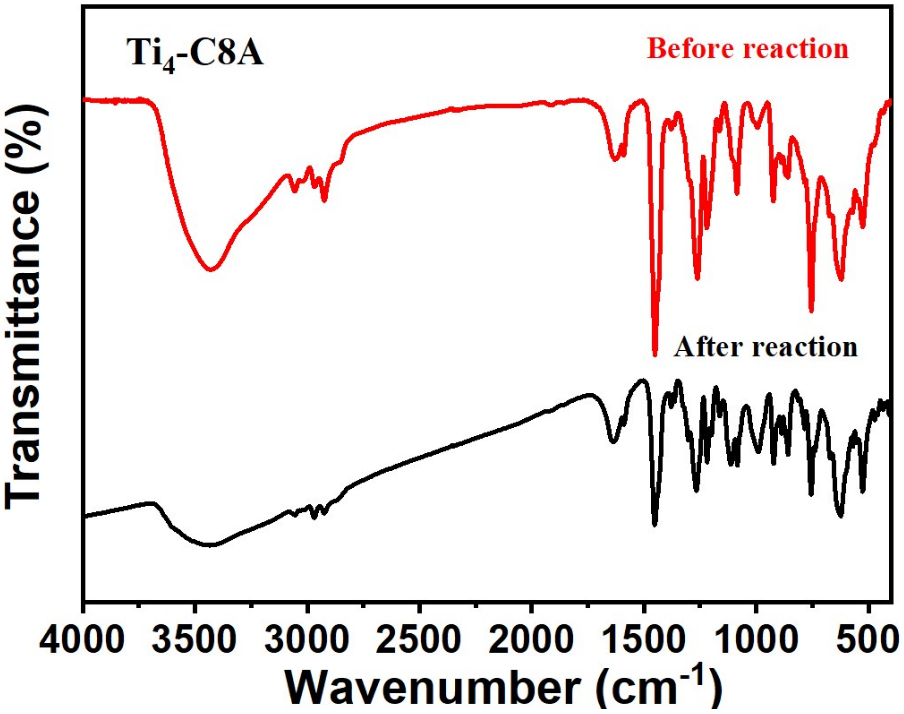

Figure S18. IR spectra of **Ti$_4$-C8A** were performed before and after the photocatalytic reaction.

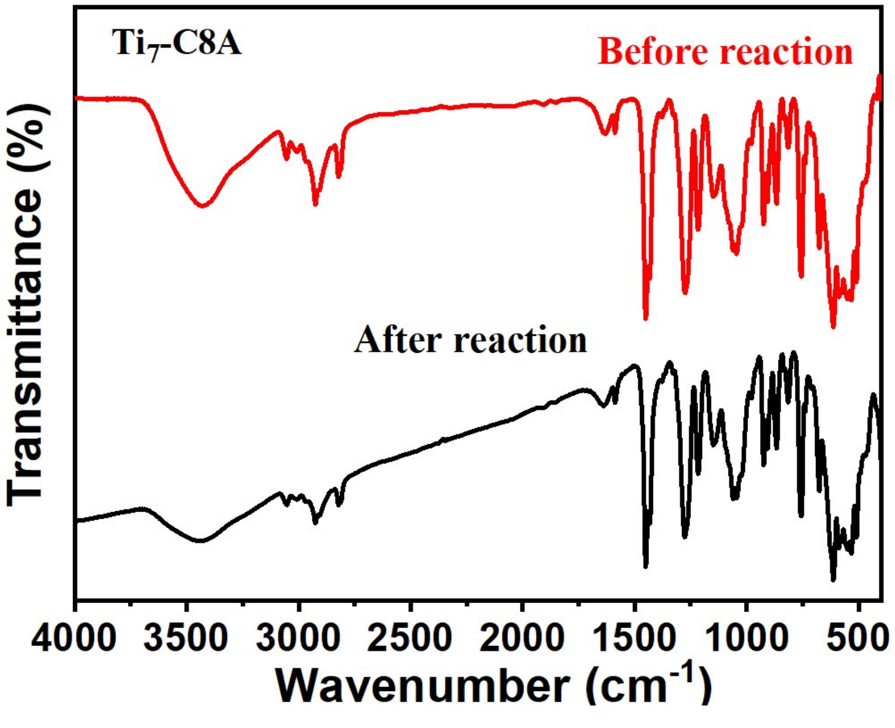

Figure S19. IR spectra of **Ti$_7$-C8A** were performed before and after the photocatalytic reaction.

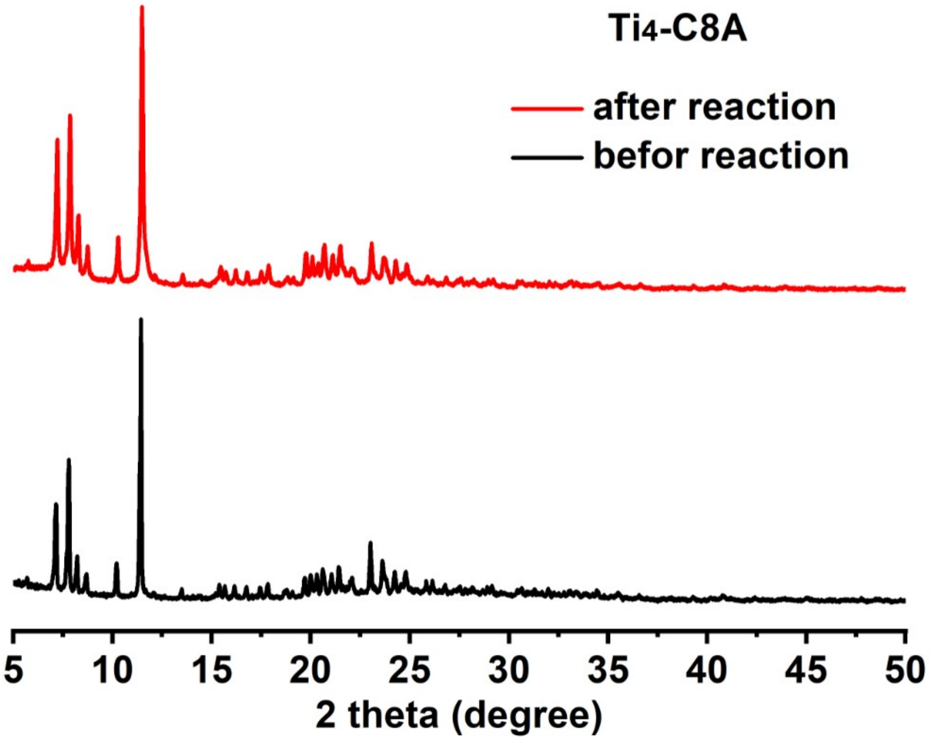

Figure S20. PXRD pattern of **Ti_4-C8A** were performed before and after the photocatalytic reaction.

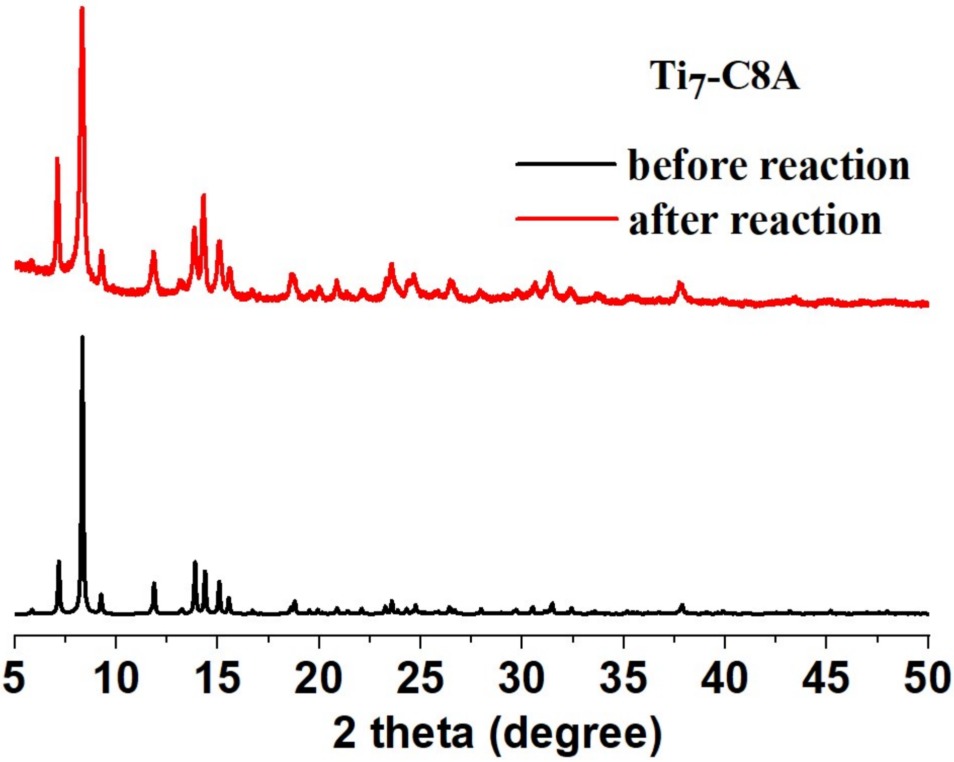

Figure S21. PXRD pattern of **Ti_7-C8A** were performed before and after the photocatalytic reaction.

Table S4. The study of photocatalytic reaction conditions[a].

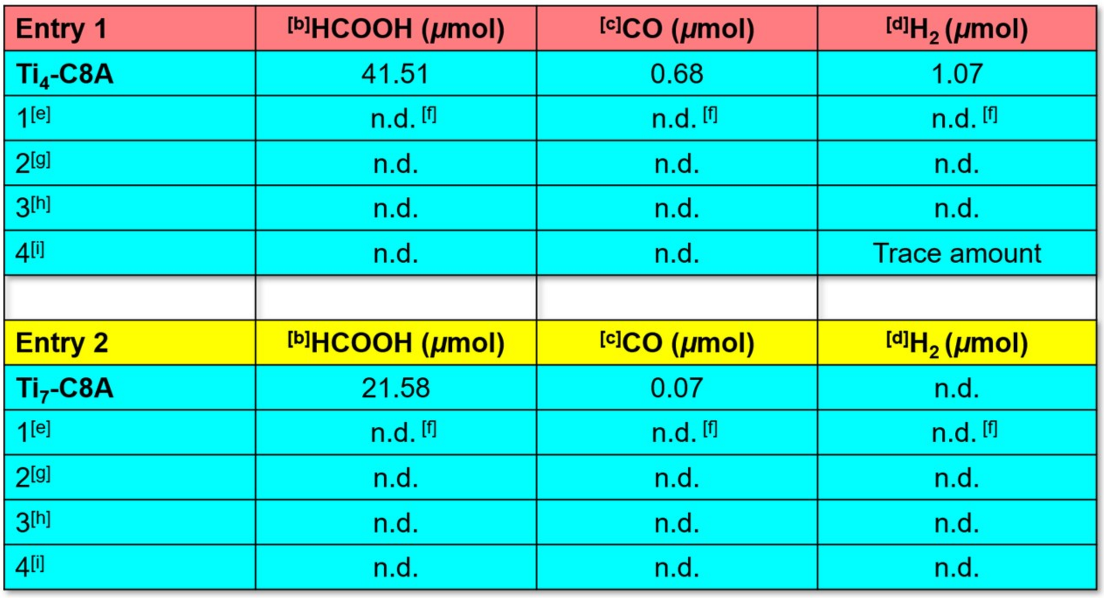

Entry 1	**[b]HCOOH (μmol)**	**[c]CO (μmol)**	**[d]H_2 (μmol)**
Ti$_4$-C8A	41.51	0.68	1.07
1[e]	n.d. [f]	n.d. [f]	n.d. [f]
2[g]	n.d.	n.d.	n.d.
3[h]	n.d.	n.d.	n.d.
4[i]	n.d.	n.d.	Trace amount
Entry 2	**[b]HCOOH (μmol)**	**[c]CO (μmol)**	**[d]H_2 (μmol)**
Ti$_7$-C8A	21.58	0.07	n.d.
1[e]	n.d. [f]	n.d. [f]	n.d. [f]
2[g]	n.d.	n.d.	n.d.
3[h]	n.d.	n.d.	n.d.
4[i]	n.d.	n.d.	n.d.

[a] Reaction conditions: catalyst (entry 1 is **Ti$_4$-C8A**, entry 2 is **Ti$_7$-C8A**), H_2O (24mL), TEOA (6 mL), CO_2 (1 atm), λ = 200-400 nm (UV light), 30 °C, 17 h. [b] The HCOOH production. [c] The CO production. [d] The H_2 production. [e] In the dark. [f] Not detectable. [g] Without photocatalyst. [h] Without TEOA. [i] Using N_2 to replace CO_2.

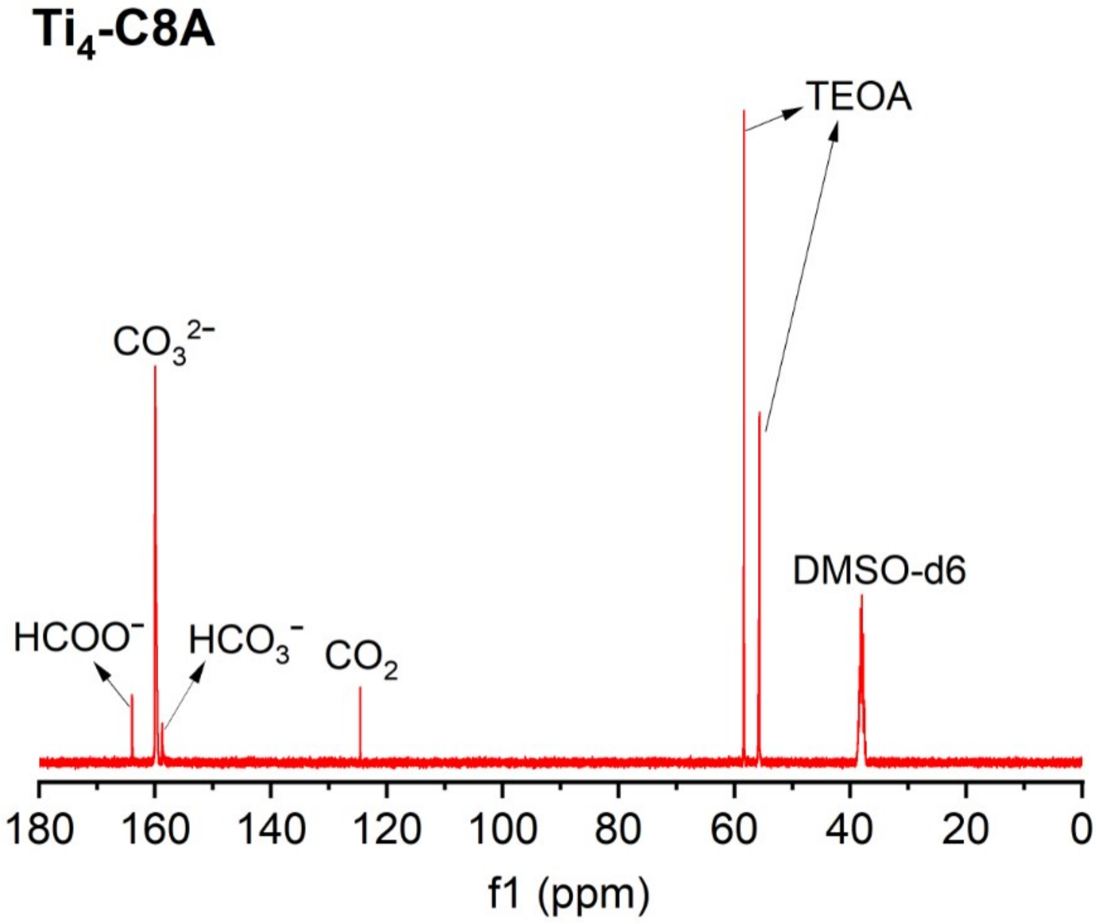

Figure S22. The ^{13}C NMR spectrum (**Ti$_4$-C8A**) for the product obtained from the reaction charging with $^{13}CO_2$. The peak at 163.9 ppm can be assigned to $HCOO^-$.

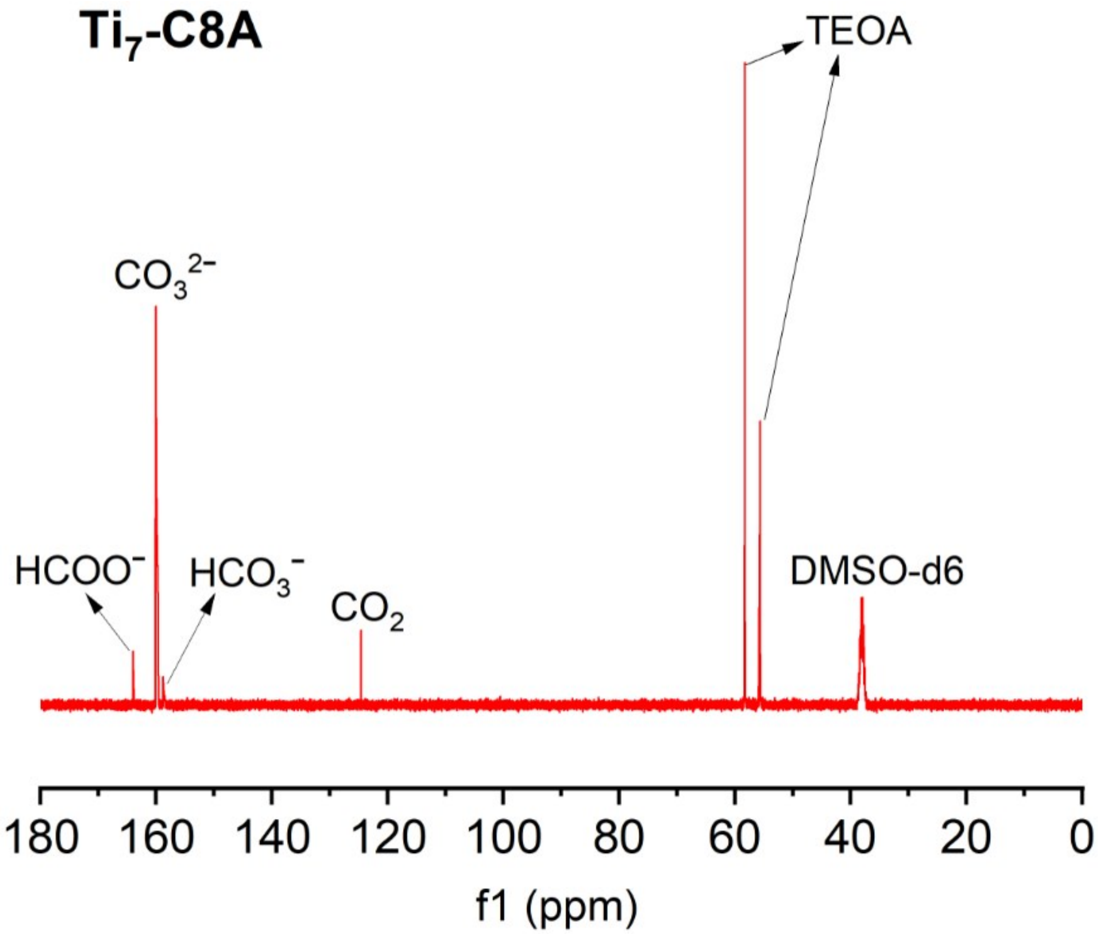

Figure S23. The ^{13}C NMR spectrum (**Ti$_7$-C8A**) for the product obtained from the reaction charging with $^{13}CO_2$. The peak at 163.9 ppm can be assigned to $HCOO^-$.

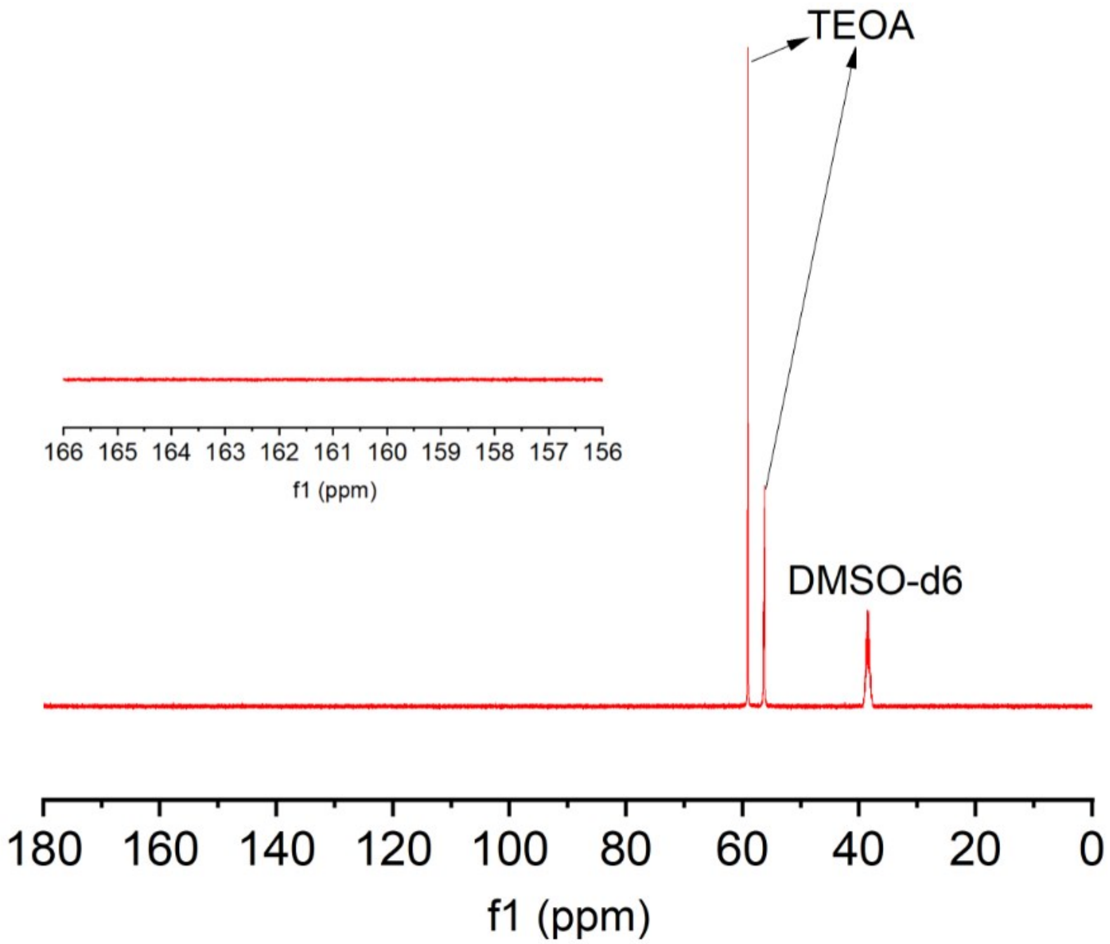

Figure S24. The ^{13}C NMR spectrum for the product obtained from the reaction charging with $^{12}CO_2$. No peak can be assigned to $HCOO^{-}$.

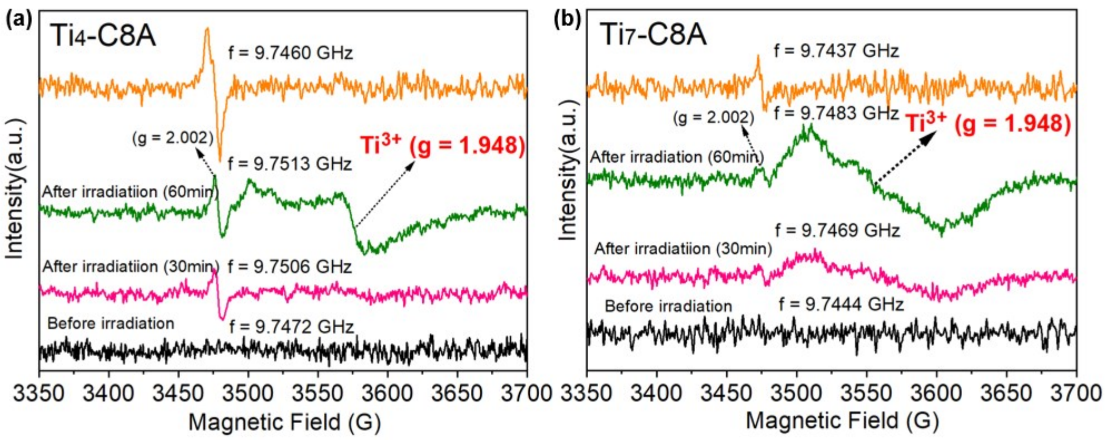

Figure S25. ESR spectra of **Ti_4-C8A** and **Ti_7-C8A** clusters before and after light irradiation. X-band Electron spin resonance (ESR) spectra were obtained on a Bruker EMX-10/12 at 298 K.

Reference

[1]. M. J. Frisch, G. W. Trucks, H. B. Schlegel, G. E. Scuseria, M. A. Robb, J. R. Cheeseman, et.al., *Gaussian 16 Rev. A.03*, Wallingford, CT, 2016.

[2]. T. Lu, F. Chen, Multiwfn: *A multifunctional wavefunction analyzer*. 2012**,** *33*, 580-592.

[3] Mele, G.; Annese, C.; D'Accolti, L.; De Riccardis, A.; Fusco, C.; Palmisano, L.; Scarlino, A.; Vasapollo, G. *Molecules* **2015**, *20*, 396-415.

[4] Gonell, F.; Puga, A. V.; Julian-Lopez, B.; Garcia, H.; Corma, *A. Appl. Catal., B* **2016**, *180*, 263-270.

[5] Chen, J. S.; Qin, S. Y.; Song, G. X.; Xiang, T. Y.; Xin, F.; Yin, X. H. *Dalton. Trans.* **2013**, *42*, 15133-15138.

[6] Jiang, W. L.; Yin, X. H.; Xin, F.; Bi, Y. D.; Liu, Y.; Li, X. *Appl. Surf. Sci*. **2014**, *288*, 138-142.

[7] Chen, J. S.; Xin, F.; Yin, X. H.; Xiang, T. Y.; Wang, Y. W. *RSC Adv*. **2015**, *5*, 3833-3839.

[8] Yang, T. C.; Chang, F. C.; Peng, C. Y.; Wang, H. P.; Wei, Y. L. *Environ. Technol*. **2015**, *36*, 2987-2990.

[9] F. Yoshitomi, K. Sekizawa, K. Maeda, O. Ishitani, *ACS Appl. Mater. Interfaces* **2015**, *7*, 13092−13097.

[10] Kuriki, R.; Sekizawa, K.; Ishitani, O.; Maeda, K. *Angew. Chem., Int. Ed*. **2015**, *54*, 2406−2409.

[11] Baran, T.; Wojtyla, S.; Dibenedetto, A.; Aresta, M.; Macyk, W. *Appl. Catal., B.* **2015**, *178*, 170−176.

[12] N. Li, J. Liu, J. J. Liu, L. Z. Dong, Z. F. Xin, Y. L. Teng, Y. Q. Lan, *Angew. Chem. Int. Ed*. **2019**, *58*, 5226 – 5231.

[13] H.-Q. Xu, J. Hu, D. Wang, Z. Li, Q. Zhang, Y. Luo, S.-H. Yu, and H.-L. Jiang. *J. Am. Chem. Soc*. **2015**, *137*, 13440−13443.

[14] Y. Fu, D. Sun, Y. Chen, R. Huang, Z. Ding, X. Fu, and Z. Li. *Angew. Chem. Int. Ed.* **2012**, *51*, 3364 –3367.

[15] D. Wang, R. Huang, W. Liu, D. Sun, and Z. Li. *ACS Catal*. **2014**, *4*, 4254−4260.

[16] Y. Lee, S. Kim, J. K. Kang and S. M. Cohen. *Chem. Commun*., **2015**, *51*, 5735—5738.

[17] D. Sun, W. Liu, M. Qiu, Y. Zhang, Z. Li. *Chem. Commun.*, **2015**, *51*, 2056-2059.

[18] D. Sun, Y. Fu, W. Liu, L. Ye, D. Wang, L. Yang, X. Fu, and Z. Li. *Chem. Eur. J*. **2013**, *19*, 14279 – 14285.

[19] D. Chen, H. Xing, C. Wang and Z. Su. *J. Mater. Chem. A*, **2016**, *4*, 2657–2662.

[20] D. R. Sun, Y. H. Gao, J. L. Fu, X. C. Zeng, Z. N. Chen, Z. H. Li, *Chem. Commun*. **2015**, *51*, 2645−2648.

[21] (a) S. Q. Zhang, L. N. Li, S. G. Zhao, Z. H. Sun, J. H. Luo, *Inorg. Chem.* **2015**, *54*, 8375−8379; (b) S. Q. Zhang, L. N. Li, S. E. Zhao, Z. H. Sun, M. C. Hong, J. H. Luo, *J. Mater. Chem. A*. **2015**, *3*, 15764−15768.